LETTER

doi:10.1038/nature14593

Eye-like ocelloids are built from different endosymbiotically acquired components

Gregory S. Gavelis[1], Shiho Hayakawa[1,2,3], Richard A. White III[4]†, Takashi Gojobori[3,5], Curtis A. Suttle[2,4,6,7], Patrick J. Keeling[2,7] & Brian S. Leander[1,2,7]

Multicellularity is often considered a prerequisite for morphological complexity, as seen in the camera-type eyes found in several groups of animals. A notable exception exists in single-celled eukaryotes called dinoflagellates, some of which have an eye-like 'ocelloid' consisting of subcellular analogues to a cornea, lens, iris, and retina[1]. These planktonic cells are uncultivated and rarely encountered in environmental samples, obscuring the function and evolutionary origin of the ocelloid. Here we show, using a combination of electron microscopy, tomography, isolated-organelle genomics, and single-cell genomics, that ocelloids are built from pre-existing organelles, including a cornea-like layer made of mitochondria and a retinal body made of anastomosing plastids. We find that the retinal body forms the central core of a network of peridinin-type plastids, which in dinoflagellates and their relatives originated through an ancient endosymbiosis with a red alga[2]. As such, the ocelloid is a chimaeric structure, incorporating organelles with different endosymbiotic histories. The anatomical complexity of single-celled organisms may be limited by the components available for differentiation, but the ocelloid shows that pre-existing organelles can be assembled into a structure so complex that it was initially mistaken for a multicellular eye[3]. Although mitochondria and plastids are acknowledged chiefly for their metabolic roles, they can also be building blocks for greater structural complexity.

Many organisms can orient to light. In some single-celled eukaryotes, such as *Chlamydomonas* and many dinoflagellates, an 'eyespot' directs photons onto photoreceptors on the flagellum, allowing the cell to respond to the intensity and direction of light[4,5]. A vastly more complex structure is found in warnowiid dinoflagellates: the eye-like ocelloid. Ocelloids consist of subcellular components resembling a lens, a cornea, iris-like rings, and a pigmented cup called the retinal body[6–9], which together so resemble the camera-type eyes of some animals that they have been speculated to be homologous[10] (Figs 1 and 2). The first description of a warnowiid was dismissed as a cell that had scavenged the eye from a jellyfish[3]. Ultrastructural studies of the ocelloid subsequently suggested that the retinal body might be derived from a plastid, in that it contains thylakoid-like membranes during cell division[4,8,9].

The ocelloid is among the most complex subcellular structures known, but its function and evolutionary relationship to other organelles remain unclear. This poor state of knowledge can be attributed to the fact that warnowiids are uncultivated and rarely encountered in environmental samples, with as few as two cells reported from the plankton per year for some species[11]. Modern single-cell genomics and microscopy approaches, however, provide opportunities to study uncultivated eukaryotes at the molecular and ultrastructural levels, including rare species[12–14]. In an attempt to learn more about the cell biology of ocelloids, we applied single-cell transcriptomics to two genera of warnowiids: *Erythropsidinium* (Supplementary Video 1) and *Warnowia* (Supplementary Video 2), as well as transmission electron microscopy (TEM) on *Erythropsidinium* sp. and *Nematodinium* sp. Lastly, we investigated the three-dimensional ultrastructure and phylogenetic origin of the retinal body in *Nematodinium* sp. by using focused ion beam scanning electron microscopy (FIB-SEM) on isolated cells, and single-organelle genomics.

Thylakoid-like structures have been reported only once before in the retinal body[6], so we examined the ultrastructure of the ocelloid in *Nematodinium* sp. and *Erythropsidinium* sp. using single-cell TEM. During interphase, the retinal body contains highly ordered waveform membranes (Fig. 2), which are perpendicular to the plane expected for thylakoids in a chloroplast. However, we confirmed that near the end of interphase, the waveform membranes de-differentiated into a plastid-like arrangement made of double-stacked thylakoid-like structures (Extended Data Figs 1–3). Thus, the thylakoids and waveform membranes represent two modes of the same membrane system. Moreover, we found that the retinal body of *Nematodinium* sp. exhibits red fluorescence under 505 nm (green) light—suggesting the presence of chlorophyll or another autofluorescent pigment (Extended Data Fig. 4e). In *Nematodinium*, we also found mitochondria in the ocelloid, where they formed a cornea-like layer overlying the lens (Fig. 1c and Extended Data Fig. 5)[1].

To investigate further the possible plastid origin of the retinal body, we first examined transcriptomes from isolated cells of *Erythropsidinium* sp. and *Warnowia* sp., which appear to lack photosynthetic plastids. From polyadenylated complementary DNA (cDNA) libraries, we found that these heterotrophic genera expressed multiple photosynthesis-related genes (GenBank accession numbers KR632763–KR632773), including light-harvesting proteins. In addition, *Warnowia* sp. expressed three transcripts corresponding to the chloroplast-soluble peridinin–chlorophyll–binding protein, which is distinctive for dinoflagellate peridinin-type plastids[15].

The provenance of the retinal body is, however, concealed by the complex history of plastids in dinoflagellates[16]. While the ancestral peridinin-type plastid of dinoflagellates was initially acquired from a red alga, several dinoflagellates have since replaced this plastid with those from either a haptophyte, a cryptophyte, a diatom, or a green alga, and several non-photosynthetic lineages have been found to possess relict plastids[2,16,17]. To investigate the phylogenetic origin of the retinal body more directly, we characterized genes encoded on DNA associated with the organelle structures. Single cells of *Nematodinium* sp. were micro-dissected, and individual retinal bodies were isolated (Fig. 1). Retinal bodies were washed three times, as contaminant DNA can be a confounding factor in any genomic study. The individual retinal bodies from five cells were pooled, lysed, and their DNA was amplified with phi29 polymerase through multiple displacement amplification. To compare the DNA content of dissected organelles with the DNA content of whole *Nematodinium* cells (including nuclei), we

[1]Department of Zoology, University of British Columbia, Vancouver, British Columbia V6T 1Z4, Canada. [2]Department of Botany, University of British Columbia, Vancouver, British Columbia V6T 1Z4, Canada. [3]Center for Information Biology, National Institute of Genetics, Mishima, Shizuoka 411-8540, Japan. [4]Department of Microbiology and Immunology, University of British Columbia, Vancouver, British Columbia V6T 1Z4, Canada. [5]Computational Bioscience Research Center, King Abdullah University of Science and Technology, Thuwal 23955-6900, Saudi Arabia. [6]Department of Earth, Ocean and Atmospheric Sciences, University of British Columbia, Vancouver, British Columbia V6T 1Z4, Canada. [7]Canadian Institute for Advanced Research, Toronto, Ontario M5G 1Z8, Canada.
†Present address: Biological Sciences Division, Pacific Northwest National Laboratory, Richland, Washington 99354, USA.

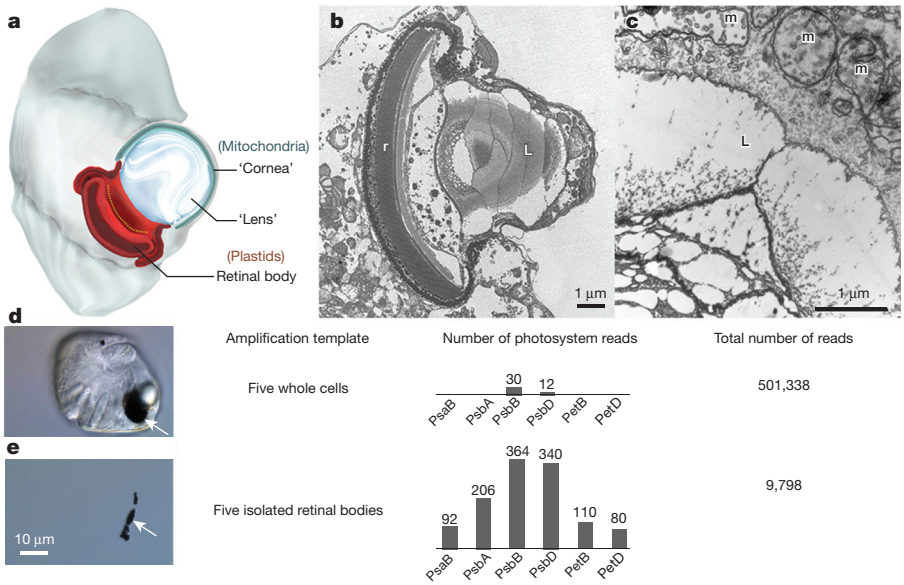

Figure 1 | Genomics and structure of organelles in the ocelloid. **a**, Illustration of *Nematodinium* showing the basic components of the ocelloid with their putative organellar origins. **b**, TEM of the ocelloid of *Erythropsidinium*, including the lens (L) and retinal body (r). **c**, TEM of the ocelloid of *Nematodinium*, depicting the edge of the lens (L) where it is overlain by a cornea-like layer of mitochondria (m). **d**, Genomic reads amplified from five whole cells of *Nematodinium*; arrow, retinal body. **e**, Genomic reads amplified from five retinal bodies (arrow) after they were micro-dissected from individual cells of *Nematodinium*.

also pooled five intact *Nematodinium* sp. cells and subjected them to the same procedures for DNA amplification and sequencing. From sequence databases derived from both samples, we identified genes that are encoded in the plastid of other dinoflagellates. Overall, six plastid genes were identified from isolated retinal bodies, *PsaB*, *PsbA*, *PsbB*, *PsbD*, *PetB*, and *PetD*, spanning photosystems I and II. These genes grouped strongly with the peridinin-containing plastids of dinoflagellates in individual and concatenated phylogenetic analysis (Fig. 3 and Extended Data Figs 6 and 7), and, collectively, plastid-encoded genes represented 13% of all reads. By contrast, the proportion of plastid/nuclear DNA in the whole-cell amplification was less than 0.0001%. The representation of plastid DNA in the retinal body was, therefore, over 1,600-fold higher than in whole cells (Fig. 1). While *in situ* hybridization is required to conclude firmly that plastid genomic DNA is localized within the retinal body, our findings strongly suggest that the retinal body is associated with a plastid genome.

Although the genomic data suggest that the retinal body is a derived plastid, there is another potential source of plastid DNA within the cell. Our isolates of *Nematodinium* contained small brown-pigmented bodies with double-stacked thylakoids typical of peridinin-type plastids. The presence of these plastids in addition to the retinal body raises the possibility that *Nematodinium* has two different morphotypes of peridinin plastid within the same cell. However, the physical relationship between these plastid types was unclear from TEM alone, and the retinal body retains a distinct pigmentation as well as producing daughter retinal bodies through binary fission[6,8].

To investigate the physical connections between the different components of the ocelloid and surrounding structures, such as peridinin-type plastids, we performed FIB-SEM tomography on a single isolated cell of *Nematodinium* sp. The three-dimensional reconstructions of our FIB-SEM data demonstrated that the outer membrane of the retinal body is fused to a network of adjacent plastids, forming a membranous web throughout the cell (Fig. 4, Extended Data Fig. 8 and Supplementary Video 3). Therefore, the retinal body appears to be a differentiated region of a larger, netlike plastid. The fact that this plastid network was not evident in previous TEM-based studies of *Nematodinium*[18] suggests that hidden organelle networks could be widely overlooked in nature. Functional differentiation of discrete regions of plastids is known in other contexts, such as the pyrenoid—a centralized carbon-fixing region in many plastids—or the eyespots of some other eukaryotes, which consist of an intra-plastidial pigment cluster facing the flagellum[4,5].

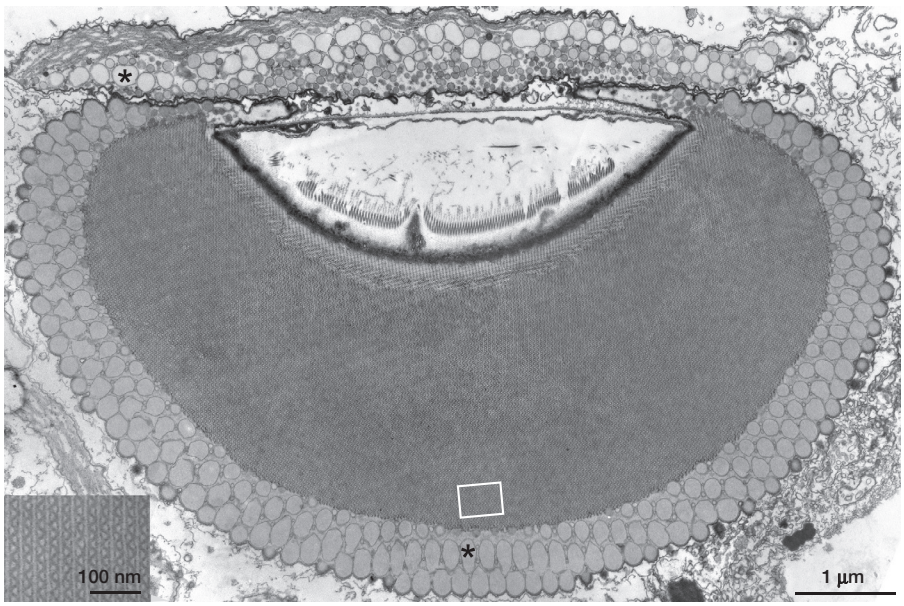

Figure 2 | Ultrastructure of the retinal body in *Nematodinium* sp. A composite of 12 electron micrographs showing a glancing section through the retinal body, which contains stacked waveform membranes (white square and inset) enveloped by pigmented lipid droplets (asterisk). Scale bar, 1 µm.

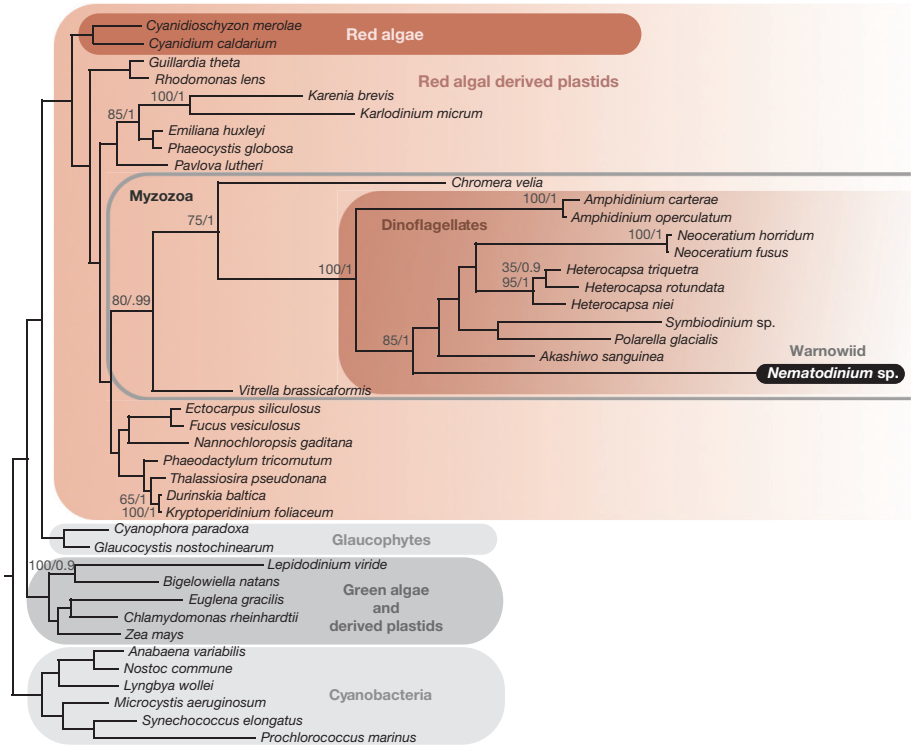

Figure 3 | Phylogeny of retinal-body-encoded proteins. Six partial plastid genes from the retinal body of the ocelloid in *Nematodinium* sp. were amplified. Photosystem I P700 apoprotein A2, photosystem II protein D1, photosystem II CP47 protein, photosystem II protein D1, cytochrome b_6, and cytochrome b_6/f complex subunit 4 were translated and concatenated for a 1,618-amino-acid alignment. The tree was inferred by analysing the 42-taxon alignment using maximum likelihood. Statistical support for the branches was evaluated using 500 maximum likelihood bootstrap replicates and Bayesian posterior probabilities. Support values are shown for all branches within the Myzozoa (dinoflagellates and chromerids).

Tomographic reconstructions also confirmed a close association between mitochondria and the lens of the ocelloid. The mitochondria surrounding the lens were interconnected and formed a sheet-like 'cornea' layer consistent with TEM data. The corneal layer surrounded all regions of the lens except for a few minor perforations and the side facing the retinal body (Fig. 4). The corneal mitochondria appear to form a continuous network with mitochondria in the nearby cytoplasm. The ocelloid, therefore, represents an intriguing mixture of components with endogenous and endosymbiotic origins.

Before this study, there was little evidence for homology between the ocelloid and other structures found in dinoflagellates[4]. On the basis of its resemblance to camera-type eyes, a relationship was even suggested between the ocelloid and the eyes of some animals[10]. To the contrary, our findings indicate that the ocelloid is a conglomerate of several membrane-bound organelles, including endomembrane vesicles, mitochondria, and plastids. The ocelloid is probably homologous to the much simpler eyespots found in several other lineages of dinoflagellates (Extended Data Fig. 9), most of which share features in

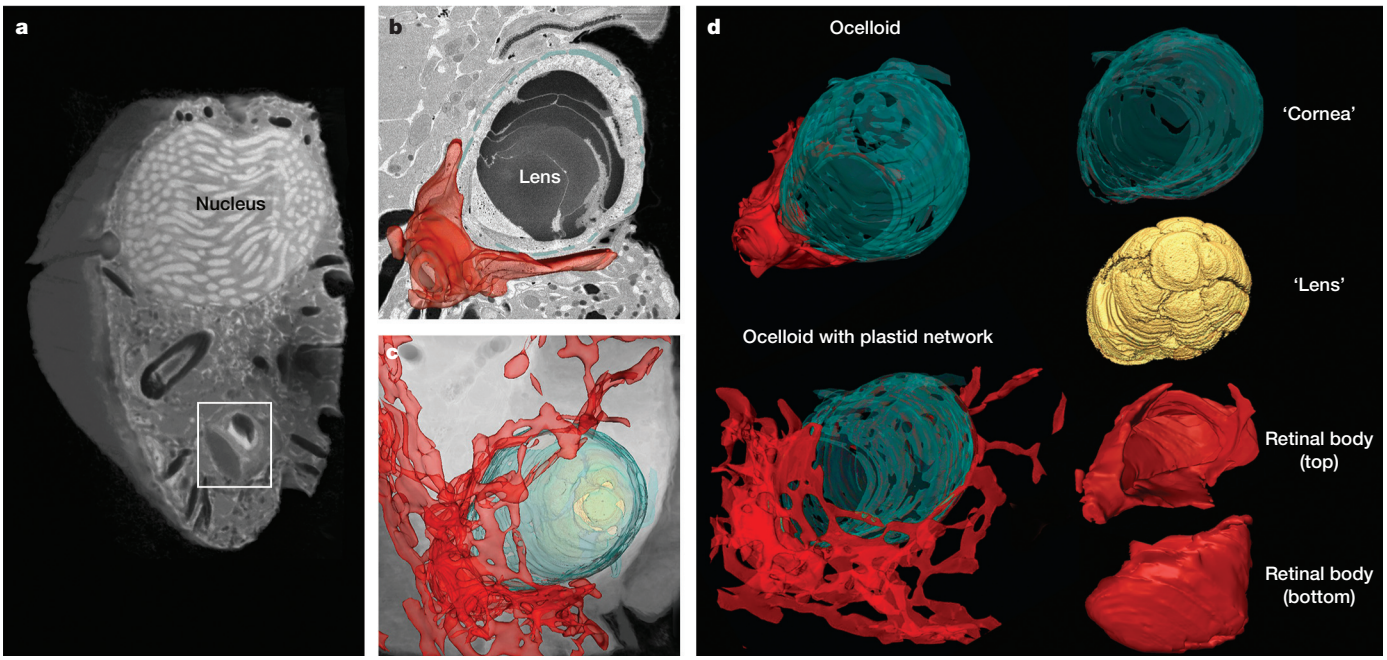

Figure 4 | Three-dimensional reconstruction of the ocelloid of *Nematodinium* sp. using FIB-SEM tomography. **a**, Stack of a halved cell, showing the nucleus and the ocelloid (box). **b**, FIB-SEM slice of the ocelloid, depicting the lens, mitochondria (blue), and retinal body (red). **c**, Translucent FIB-SEM stack of the region surrounding the ocelloid, including the lens (yellow) and full plastid network (red). **d**, Reconstructions of the ocelloid and its component parts, including the mitochondrial cornea-like layer, vesicular lens, and retinal body.

common with the peridinin plastid[4,19,20]. Peridinin plastids stem from an ancient red alga that was incorporated by the common ancestor of all myzozoans (dinoflagellates, chromerids, and apicomplexans), many of which (including all apicomplexans) subsequently lost photosynthesis and reduced their plastids to cryptic, morphologically simple structures[2,16]. While morphological reduction is a common trend among endosymbiotic organelles, the ocelloid in warnowiids demonstrates that increased complexity can also arise.

To understand the function of the ocelloid, a basic knowledge of the life history of warnowiid dinoflagellates is required. Understanding warnowiid behaviour is a difficult problem, however, because their cells are rarely encountered, have never been cultivated, and degrade rapidly when removed from the plankton[11]. Nevertheless, we observed one important detail of warnowiid life history using TEM of individual cells isolated directly from the ocean. We found that the food vacuoles in *Nematodinium* contained trichocysts (Extended Data Fig. 10), which are defensive extrusive organelles found in dinoflagellates[21]. These data suggest that *Nematodinium* feeds on other dinoflagellates, so one hypothesis is that the ocelloid is involved in the detection of other dinoflagellates as prey. Some dinoflagellates are capable of bioluminescence[22], which may be what ocelloids detect, but all dinoflagellates contain a distinctively large nucleus of permanently condensed chromosomes, and these chromosomes polarize light[23]. An intriguing possibility is that the ocelloid can detect polarized light, and, by extension, preferred prey. Testing such a specific phototactic behaviour will be challenging until warnowiids are brought into culture. Nevertheless, the genomic and detailed ultrastructural data presented here have resolved the basic components of the ocelloid and their origins, and demonstrate how evolutionary plasticity of mitochondria and plastids can generate an extreme level of subcellular complexity.

Online Content Methods, along with any additional Extended Data display items and Source Data, are available in the online version of the paper; references unique to these sections appear only in the online paper.

Received 12 February 2015; accepted 22 May 2015.
Published online 1 July 2015.

1. Greuet, C. Organisation ultrastructurale de l'ocelle de deux Peridiniens Warnowiidae, *Erythropsis pavillardi* Kofoid et Swezy et *Warnowia pulchra* Schiller. *Protistologica* **4,** 209–230 (1968).
2. Janouskovec, J. *et al.* A common red algal origin of the apicomplexan, dinoflagellate, and heterokont plastids. *Proc. Natl Acad. Sci. USA* **107,** 10949–10954 (2010).
3. Kofoid, C. A. & Swezy, O. The free-living, unarmoured dinoflagellates. *Mem. Univ. Calif.* **5,** 1–562 (1921).
4. Dodge, J. D. The functional and phylogenetic significance of dinoflagellate eyespots. *Biosystems* **16,** 259–267 (1984).
5. Kreimer, G. Reflective properties of different eyespot types in dinoflagellates. *Protist* **150,** 311–323 (1999).
6. Greuet, C. Structural and ultrastructural evolution of ocelloid of *Erythropsidinium-pavillardi*, Kofoid-and-Swezy (dinoflagellate Warnowiidae, Lindemann) during division and palintomic divisions. *Protistologica* **13,** 127–143 (1977).
7. Greuet, C. Structure fine de locelle d'*Erythropsis pavillardi* Hertwig, peridinien Warnowiidae Lindemann. *C.R. Acad. Sci.* **261,** 1904–1907 (1965).
8. Hoppenrath, M. *et al.* Molecular phylogeny of ocelloid-bearing dinoflagellates (Warnowiaceae) as inferred from SSU and LSU rDNA sequences. *BMC Evol. Biol.* **9,** 116 (2009).
9. Leander, B. S. Different modes of convergent evolution reflect phylogenetic distances. *Trends Ecol. Evol.* **23,** 481–482 (2008).
10. Gehring, W. J. New perspectives on eye development and the evolution of eyes and photoreceptors. *J. Hered.* **96,** 171–184 (2005).
11. Gomez, F., Lopez-Garcia, P. & Moreira, D. Molecular phylogeny of the ocelloid-bearing dinoflagellates *Erythropsidinium* and *Warnowia* (Warnowiaceae, Dinophyceae). *J. Eukaryot. Microbiol.* **56,** 440–445 (2009).
12. Yoon, H. S. *et al.* Single-cell genomics reveals organismal interactions in uncultivated marine protists. *Science* **332,** 714–717 (2011).
13. Lasken, R. S. Genomic sequencing of uncultured microorganisms from single cells. *Nature Rev. Microbiol.* **10,** 631–640 (2012).
14. Kolisko, M. *et al.* Single-cell transcriptomics for microbial eukaryotes. *Curr. Biol.* **24,** R1081–R1082 (2014).
15. Hofmann, E. *et al.* Structural basis of light harvesting by carotenoids: peridinin-chlorophyll-protein from *Amphidinium carterae*. *Science* **272,** 1788–1791 (1996).
16. Keeling, P. J. The number, speed, and impact of plastid endosymbioses in eukaryotic evolution. *Annu. Rev. Plant Biol.* **64,** 583–607 (2013).
17. Saldarriaga, J. F. *et al.* Dinoflagellate nuclear SSU rRNA phylogeny suggests multiple plastid losses and replacements. *J. Mol. Evol.* **53,** 204–213 (2001).
18. Mornin, L. & Francis, D. Fine structure of *Nematodinium armatum*, a naked dinoflagellate. *J. Microsc.* **6,** 759–772 (1967).
19. Lindberg, K., Moestrup, O. & Daugbjerg, N. Studies on woloszynskioid dinoflagellates I: *Woloszynskia coronata* re-examined using light and electron microscopy and partial LSU rDNA sequences, with description of *Tovellia* gen. nov. and *Jadwigia* gen. nov. (Tovelliaceae fam. nov.). *Phycologia* **44,** 416–440 (2005).
20. Moestrup, O., Hansen, G. & Daugbjerg, N. Studies on woloszynskioid dinoflageflates III: on the ultrastructure and phylogeny of *Borghiella dodgei* gen. et sp nov., a cold-water species from Lake Tovel, N. Italy, and on *B. tenuissima* comb. nov. (syn. *Woloszynskia tenuissima*). *Phycologia* **47,** 54–78 (2008).
21. Hausmann, K. Extrusive organelles in protists. *Int. Rev. Cytol.* **52,** 197–276 (1978).
22. Abrahams, M. V. & Townsend, L. D. Bioluminescence in dinoflagellates: a test of the burglar alarm hypothesis. *Ecology* **74,** 258–260 (1993).
23. Liu, J. & Kattawar, G. W. Detection of dinoflagellates by the light scattering properties of the chiral structure of their chromosomes. *J. Quant. Spectrosc. Radiat. Transf.* **131,** 24–33 (2013).

Supplementary Information is available in the online version of the paper.

Acknowledgements This work was supported by grants from the Natural Sciences and Engineering Research Council of Canada (2014-05258 to B.S.L., and 227301 to P.J.K.) and the Tula Foundation (Centre for Microbial Diversity and Evolution). We thank G. Owen for his operation of the FIB-SEM and G. Martens for preparing our samples for tomography. G.S.G. thanks S. Maslakova, C. Young, A. Lehman, and D. Blackburn for training in developmental biology, marine systems, electron microscopy, and ultrastructure, respectively. C.A.S., P.J.K. and B.S.L. are Senior Fellows of the Canadian Institute for Advanced Research.

Author Contributions G.S.G., S.H., P.J.K. and B.S.L. designed the experiments. G.S.G. performed light microscopy, TEM, FIB-SEM, dissected-organelle and single-cell genomics, and phylogenetic analyses on specimens he collected in Canada, with resources and funding from B.S.L. and P.J.K. S.H. performed light microscopy, TEM, and transcriptomics on specimens she collected in Japan with resources and funding from T.G., and was supported in Canada by P.J.K. and B.S.L. R.A.W. prepared genomic libraries for sequencing and participated in single-cell genomics with funding from C.A.S. G.S.G. and B.S.L. wrote the manuscript and all authors participated in the drafting process.

Author Information Transcriptomic data from *Warnowia* sp. and *Erythropsidinium* sp. have been deposited in GenBank under accession numbers KR632763–KR632773. Plastid genomic data from *Nematodinium* sp. have been deposited in GenBank under accession numbers KP765301–KP765306. Reprints and permissions information is available at www.nature.com/reprints. The authors declare no competing financial interests. Readers are welcome to comment on the online version of the paper. Correspondence and requests for materials should be addressed to G.G. at (zoark0@gmail.com).

METHODS

Collection. From 2005 to 2009, *Erythropsidinium* sp. and *Warnowia* sp. were collected from the marine water column in Suruga Bay (Numaza, Shizuoka), Japan. On an inverted light microscope, cells of *Erythropsidinium* sp. were identified on the basis of the presence of an ocelloid and a piston organelle (Extended Data Fig. 2b and Supplementary Video 1). Cells of *Warnowia* sp. were recognized as ocelloid-bearing cells encircled three or more times by a helical groove (Extended Data Fig. 4a and Supplementary Video 2). cDNA libraries from four cells of *Warnowia* sp. and two cells of *Erythropsidinium* sp. were prepared as described[24]. In the summer of 2012 and 2013, *Nematodinium* sp. was collected from surface water in Bamfield Inlet, Bamfield, British Columbia, Canada, with a 20 μm plankton net. Cells of *Nematodinium* sp. were identified on the basis of the presence of an ocelloid and nematocysts (Extended Data Fig. 4c). Uncultivated *Nematodinium* sp. cells containing putative prey organisms (visible as pigmented vacuoles) were chosen for TEM, so that their feeding habits could be inferred from intracellular remnants (Extended Data Fig. 10). In total, 12 cells of *Nematodinium* sp. were fixed and mounted individually for TEM, and 58 cells of *Erythropsidinium* sp. were obtained and mounted for TEM in groups.

Fluorescence and differential interference contrast microscopy. Red epifluorescence of the *Nematodinium* sp. retinal body was excited with a 505 nm argon laser on a Zeiss Axioplan inverted microscope (Extended Data Fig. 4a). Differential interference contrast observations of *Nematodinium* sp., *Warnowia* sp., and *Erythropsidinium* sp. were performed using the same microscope (Extended Data Fig. 4).

Single-cell TEM of uncultivated *Nematodinium* sp. Each isolated cell of *Nematodinium* sp. was micropipetted onto a slide coated with poly-L-lysine. Cells were fixed with 2% glutaraldehyde in filtered seawater for 30 min on ice. After two washes in filtered seawater, cells were post-fixed in 1% OsO_4 for 30 min. Cells were dehydrated through a graded series of ethanol (50%, 70%, 85%, 90%, 95%, 100%, 100%) at 10 min each, and infiltrated with a 1:1 acetone-resin mixture for 10 min. Cells were steeped in Epon 812 resin for 12 h, after which the resin was polymerized at 60 °C for 24 h to produce a resin-embedded cell affixed to the glass slide. Using a power drill, resin was shaved to a 1 mm^3 block, which was removed from the glass slide with a fine razor. The block, containing a single cell, was superglued to a resin stub in the desired orientation for sectioning. Thin (45 nm) sections were produced with a diamond knife, post-stained with uranyl acetate and lead citrate, and viewed under a Hitachi H7600 TEM.

Isolation of the retinal bodies of *Nematodinium* sp. In preparation for single-organelle genomics, five cells of *Nematodinium* sp. with no visible prey contents were selected to minimize the chances of genetic contamination. Each cell of *Nematodinium* was micropipetted onto a slide in a droplet of TE buffer and affixed to a patch of poly-L-lysine. Cells were lysed with nuclease-free water. The nucleus and other cell contents were gently dislodged with rinses of TE buffer, leaving the retinal body behind for manual isolation (Fig. 1d). Unlike the retinal body, which is darkly pigmented, the cornea and mitochondria of the ocelloid are much smaller, transparent, and could not be isolated after cell lysis or tracked through rinse steps. Five different retinal bodies were isolated and pooled onto a new, sterile slide, and washed three times with TE buffer to remove as many other cellular remnants as possible.

Single-organelle genomics of *Nematodinium* sp. To test for the presence of a plastid genome in the retinal body, we performed a genomic amplification using phiX 29 polymerase (Repli-G mini kit, Qiagen) on five individually isolated retinal bodies that were then pooled together. We performed a control reaction by amplifying a pool of five whole cells of *Nematodinium* sp. using the same procedures as for the retinal bodies. The whole-cell amplification provided a measure of overall plastid DNA concentration, against which the retinal body plastid DNA concentration could be compared. To minimize amplification bias, each reaction was divided into four aliquots, run in parallel, and pooled after the 15 h amplification period. Paired end sequencing on an Illumina MiSeq yielded 9,798 reads from the retinal bodies, versus 501,338 reads from whole cells. From these reads, plastid genes were assembled using the *de novo* assembly program Ray[25], which fragmented the reads into a variety of hash sizes ('kmers'), then assembled them. We found the assembly from 53 base pair (bp) kmers to be optimal, recovering six partial plastid genes (Fig. 1d, e). To estimate the concentration of plastid reads in the whole cell versus isolated retinal body amplifications, we counted plastid reads in Bowtie[26], a read mapping program, then divided them by the total number of reads sequenced from that reaction (Fig. 1d, e).

Molecular phylogenetic analyses. The six plastid genes, photosystem I P700 apoprotein A2 (*PsaB*), photosystem II protein D1 (*PsbA*), photosystem II CP47 protein (*PsbB*), photosystem II protein D1 (*PsbD*), cytochrome b_6 (*PetB*), and cytochrome b_6/f complex subunit 4 (*PetD*) were translated, and their amino acids aligned with a representative set of eukaryotes in Muscle[27], with fast-evolving and ambiguously aligned regions removed in Gblocks 0.91b[28]. GenBank accession numbers are listed in Extended Data Figs 6 and 7. The amino-acid substitution model (Protein GTR gamma) was estimated from the concatenated alignment of 1,618 amino acids using the Models package in Mega 6.0.5 (ref. 29). A maximum likelihood phylogeny was run with 500 bootstraps in RAxML[30]. A second, Bayesian analysis was run for 10,000 generations in MrBayes 3.2 (ref. 31), using the high-heating setting of (nchains = 4), to account for rapid evolution of dinoflagellate plastids. These maximum likelihood analyses were run both for the multiprotein data set and for each protein individually (Extended Data Figs 6 and 7). A dinoflagellate phylogeny was estimated using 18S and 28S ribosomal DNA sequences, concatenated as 2,331 nucleotide alignment, across 36 dinoflagellate taxa including published sequences from *Nematodinium* sp., *Warnowia* sp., and *Erythropsidinium* sp. (Extended Data Fig. 6).

FIB-SEM. Cells of *Nematodinium* sp. were individually transferred into a droplet of 20% bovine serum albumin in phosphate buffered saline solution (an osmotically inert solution). Cells were frozen immediately to minimize fixation artefacts, using a Leica EM HPM 100 high-pressure freezer. Freeze substitution was subsequently used to remove the aqueous content of the cells and replace it with an acetone solution containing 5% water, 1% osmium tetroxide, and 0.1% uranyl acetate, at −80 °C for 48 h, −20 °C for 6 h, then graded back to 4 °C over 13 h. The prepared samples were washed twice in 100% acetone. Two cells were recovered by micropipette. Each cell was placed on a separate Thermonox coverslip, where it adhered to a patch of poly-L-lysine. In preparation for FIB-SEM, cells were infiltrated with a 1:1 mix of acetone and Embed 812 resin for 2 h, then 100% resin overnight. A second Thermonox coverslip was applied, sandwiching each cell in a thin layer of resin between the coverslips. Resin was polymerized at 65 °C for 24 h. The top coverslip was then removed with a razor blade to expose the resin face overlying the cell.

A single cell was imaged by an FEI Helios NanoLab 650 dual-beam FIB-SEM. The ion beam milled through the cell in 20 nm increments, yielding 190 image slices. Slices were aligned as a *z*-stack in Amira 5.5. Features of interest, including mitochondria and chloroplasts, were semi-automatically segmented: that is, manually traced in approximately one of every three slices, before automatic interpolation filled in the volumes between the slices. Images that did not pass quality screening because of fluctuations in microscope beam power and autofocus were not directly segmented, but were interpolated from segmentation on neighbouring images, according to the manufacturer's instructions. Surfaces of the mitochondria, chloroplasts, and vesicles were generated, smoothed, and colourized to produce a three-dimensional model of the components that form the ocelloid (Supplementary Video 3).

24. Hayakawa, S. *et al.* Function and evolutionary origin of unicellular camera-type eye structure. *PLoS ONE* **10,** http://dx.doi.org/10.1371/journal.pone.0118415 (2015).
25. Boisvert, S. *et al.* Ray: simultaneous assembly of reads from a mix of high-throughput sequencing technologies. *J. Comput. Biol.* **17,** 1519–1533 (2010).
26. Langmead, B. & Salzberg, S. Fast gapped-read alignment with Bowtie 2. *Nature Methods* **9,** 357–359 (2012).
27. Edgar, R. C. MUSCLE: Multiple sequence alignment with high accuracy and high throughput. *Nucleic Acids Res.* **32,** 1792–1797 (2004).
28. Castresana, J. Selection of conserved blocks from multiple alignments for their use in phylogenetic analysis. *Mol. Biol. Evol.* **17,** 540–552 (2000).
29. Tamura, K. *et al.* MEGA6: molecular evolutionary genetics analysis version 6.0. *Mol. Biol. Evol.* **30,** 2725–2729 (2013).
30. Stamatakis, A. RAxML-VI-HPC: maximum likelihood-based phylogenetic analyses with thousands of taxa and mixed models. *Bioinformatics* **22,** 2688–2690 (2006).
31. Ronquist, F. *et al.* MrBayes 3.2: Efficient Bayesian phylogenetic inference and model choice across a large model space. *Syst. Biol.* **61,** 539–542 (2012).

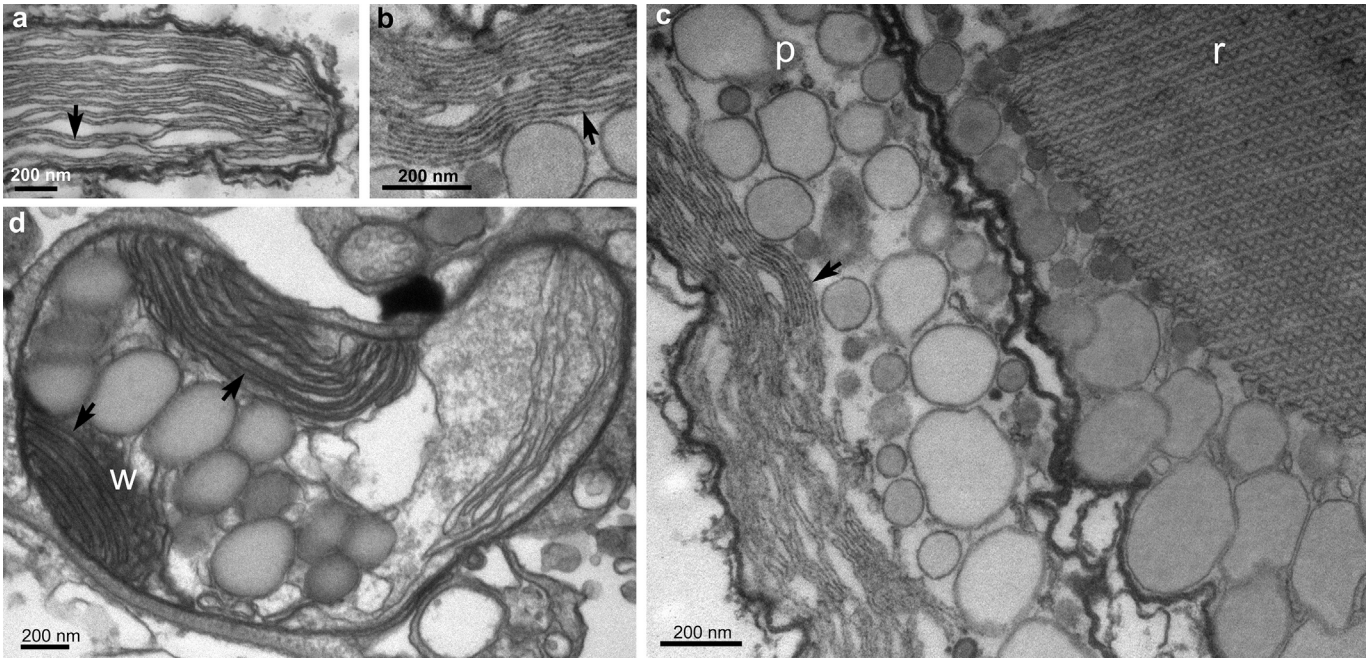

Extended Data Figure 1 | TEM of thylakoid membranes in *Nematodinium* sp. **a**, A small, peripheral plastid in *Nematodinium* sp. with typical thylakoids resembling peridinin plastids in other dinoflagellates. **b**, Thylakoids in the iris region of the ocelloid. **c**, Thylakoids in the iris positioned beside waveform membranes (w) of the retinal body, during interphase. **d**, A retinal body towards the end of interphase, in which the waveform membranes de-differentiate and are continuous with the typical thylakoids. Typical thylakoids are marked by arrows.

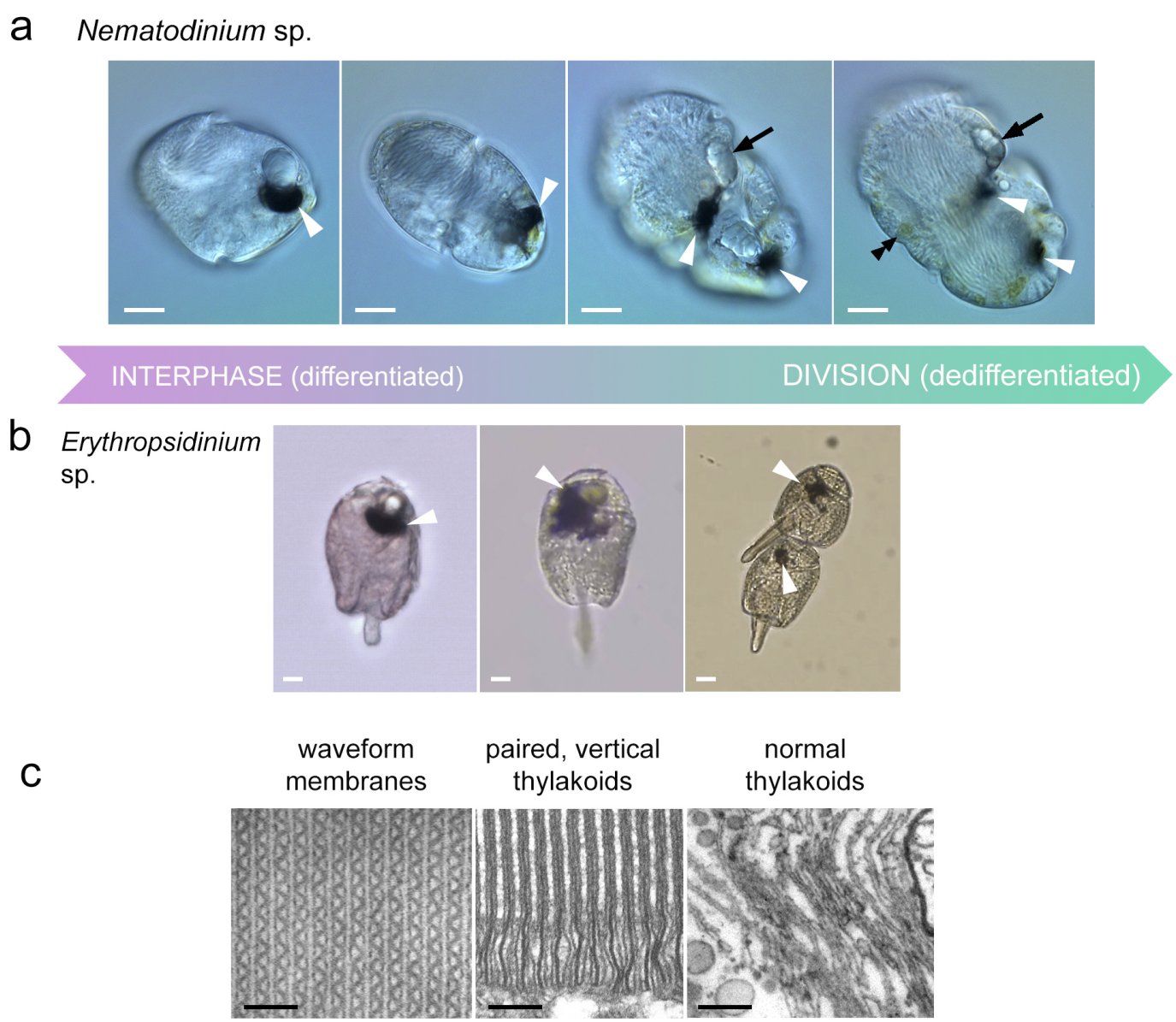

Extended Data Figure 2 | Development in warnowiids a, **b**, Light micrographs of several cells of *Nematodinium* sp., and *Erythropsidinium* sp., progressing from interphase (left) to division (right). Scale bars, 10 µm. **c**, TEM of membranes in the retinal body, during differentiated (left, *Nematodinium* sp.), transitional (middle, *Erythropsidinium* sp.), and de-differentiated modes (right, *Nematodinium* sp.). Scale bars, 200 nm. The double arrowhead marks a typical plastid; arrowheads mark the retinal bodies; arrows mark lenses that are de-differentiating.

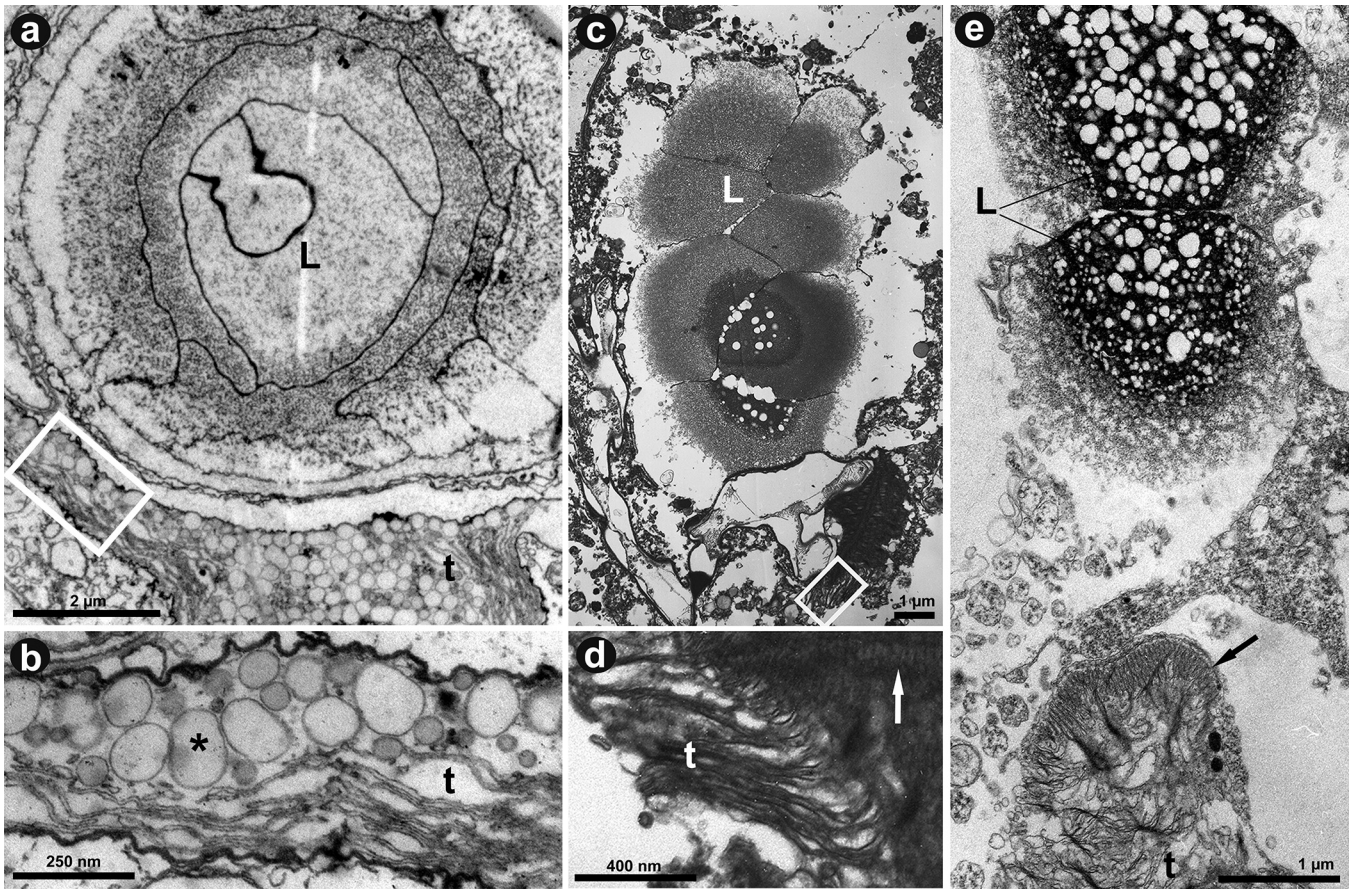

Extended Data Figure 3 | Transient thylakoids in the retinal body viewed with TEM. a, **b**, Ocelloid in a cell of *Nematodinium* sp. near division. **c**–**e**, Ocelloid in cells of *Erythropsidinium* sp. during division. L, lens; t, thylakoids; asterisks, lipid droplets; arrows, waveform membranes.

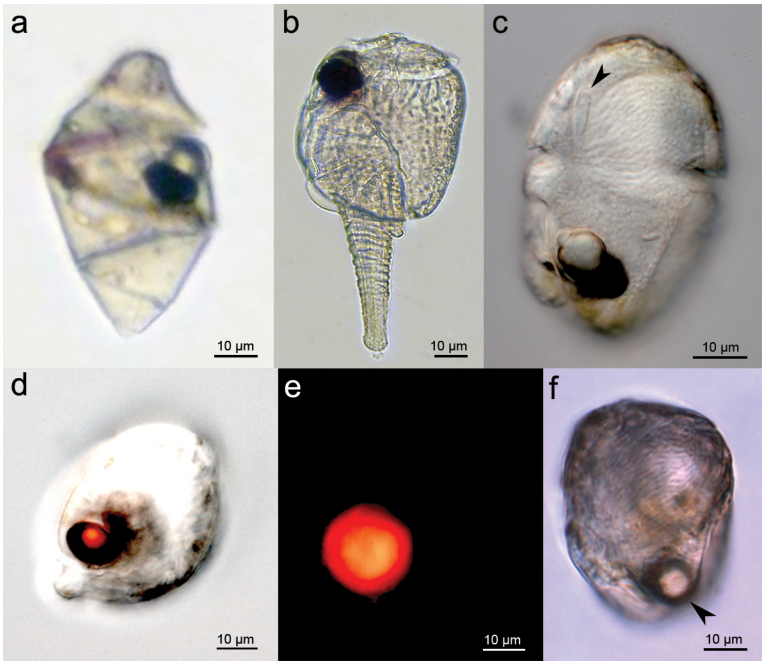

Extended Data Figure 4 | Light micrographs of warnowiids used in this study. **a**, Still frame from a video of *Warnowia* sp. **b**, *Erythropsidinium* sp. **c**, *Nematodinium* sp. with a nematocyst (arrowhead). **d**, The ventral side of *Nematodinium* sp. showing red pigmentation of the retinal body. **e**, Epifluorescence image of the same cell and angle, showing red fluorescence of the retinal body excited by 505 nm light. **f**, *Nematodinium* sp. showing a bright spot of reflectivity (that is, 'eyeshine') (arrowhead) in the ocelloid. Scale bars, 10 µm.

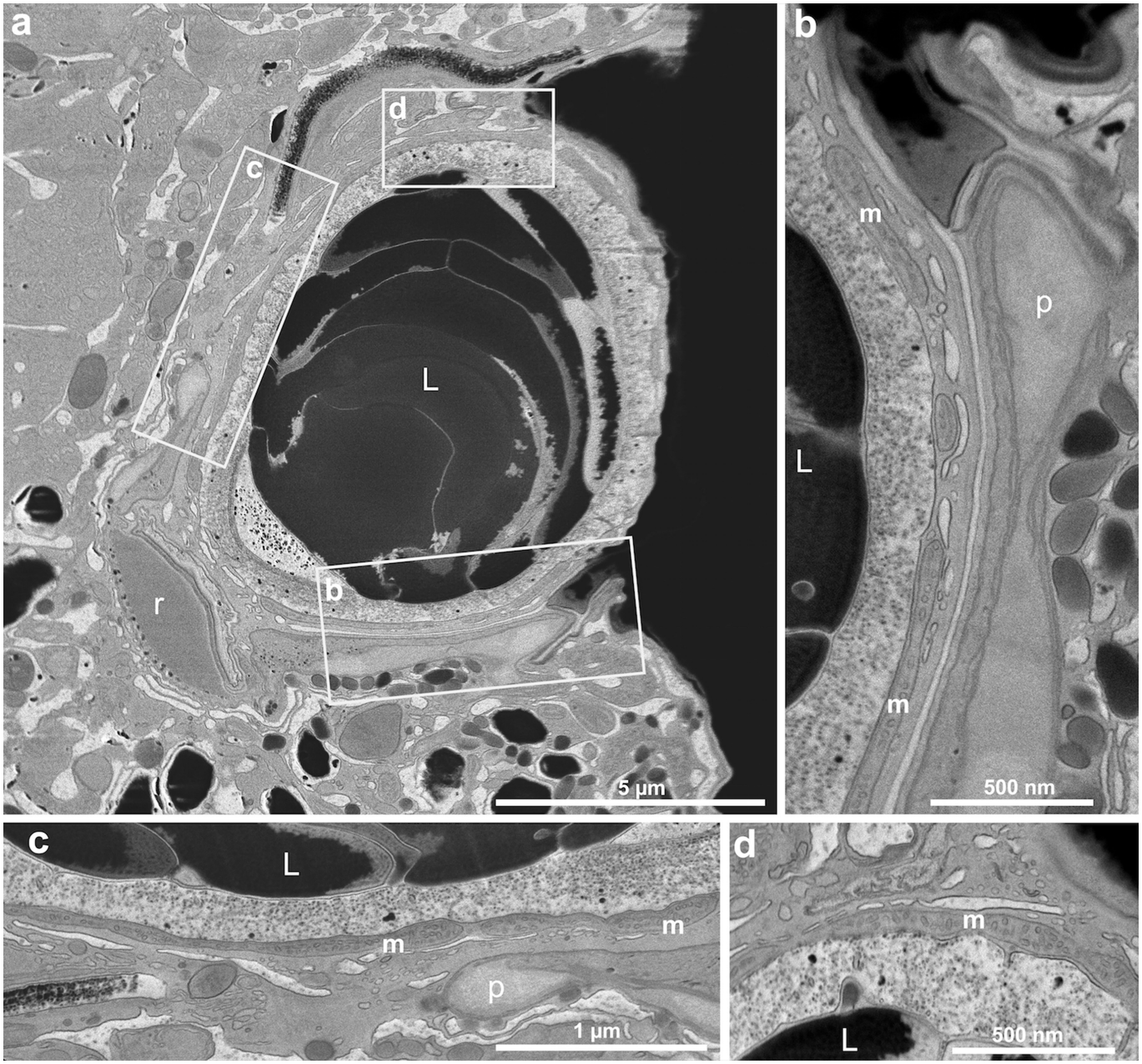

Extended Data Figure 5 | TEM of the cornea-like layer of mitochondria in the ocelloid of *Nematodinium* sp. a, Low-magnification TEM of the ocelloid, with rectangles delimiting the areas of higher magnification shown in **b**–**d**. **b**–**d**, High magnifications of structures bordering the lens (L). Mitochondria, m; pigmented ring, p; retinal body, r.

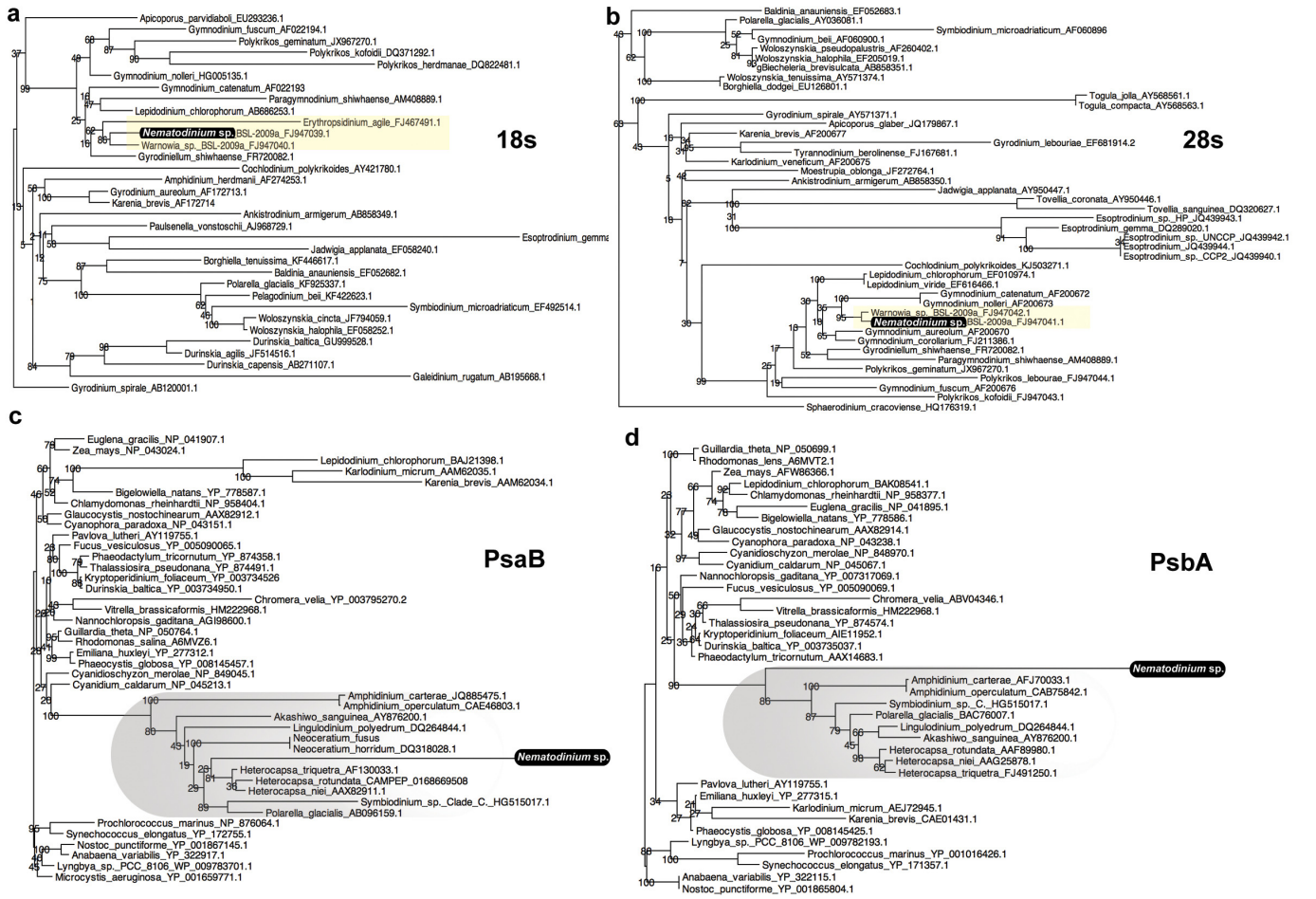

Extended Data Figure 6 | Individual ribosomal gene and photosystem protein gene trees. For **c** and **d**, the photosystem genes for *Nematodinium* sp. were amplified from the retinal body of the ocelloid. Support values for all phylogenies were calculated from 100 bootstraps using maximum likelihood analysis. **a**, 18S ribosomal DNA gene phylogeny derived from a 1,717-bp alignment across 33 dinoflagellate taxa. **b**, 28S ribosomal DNA gene phylogeny derived from a 970-bp alignment across 43 dinoflagellate taxa. For both **a** and **b**, warnowiids are highlighted in yellow and *Nematodinium* sp. is highlighted in black. **c**, Photosystem I P700 apoprotein A2 (*PsaB*) protein phylogeny derived from a 508 amino acid (AA) alignment across 42 photosynthetic taxa. **d**, Photosystem II protein D1 (*PsbA*) protein phylogeny derived from a 360 AA alignment across 39 photosynthetic taxa. For **c** and **d**, dinoflagellates are shaded in grey, and *Nematodinium* sp. is highlighted in black.

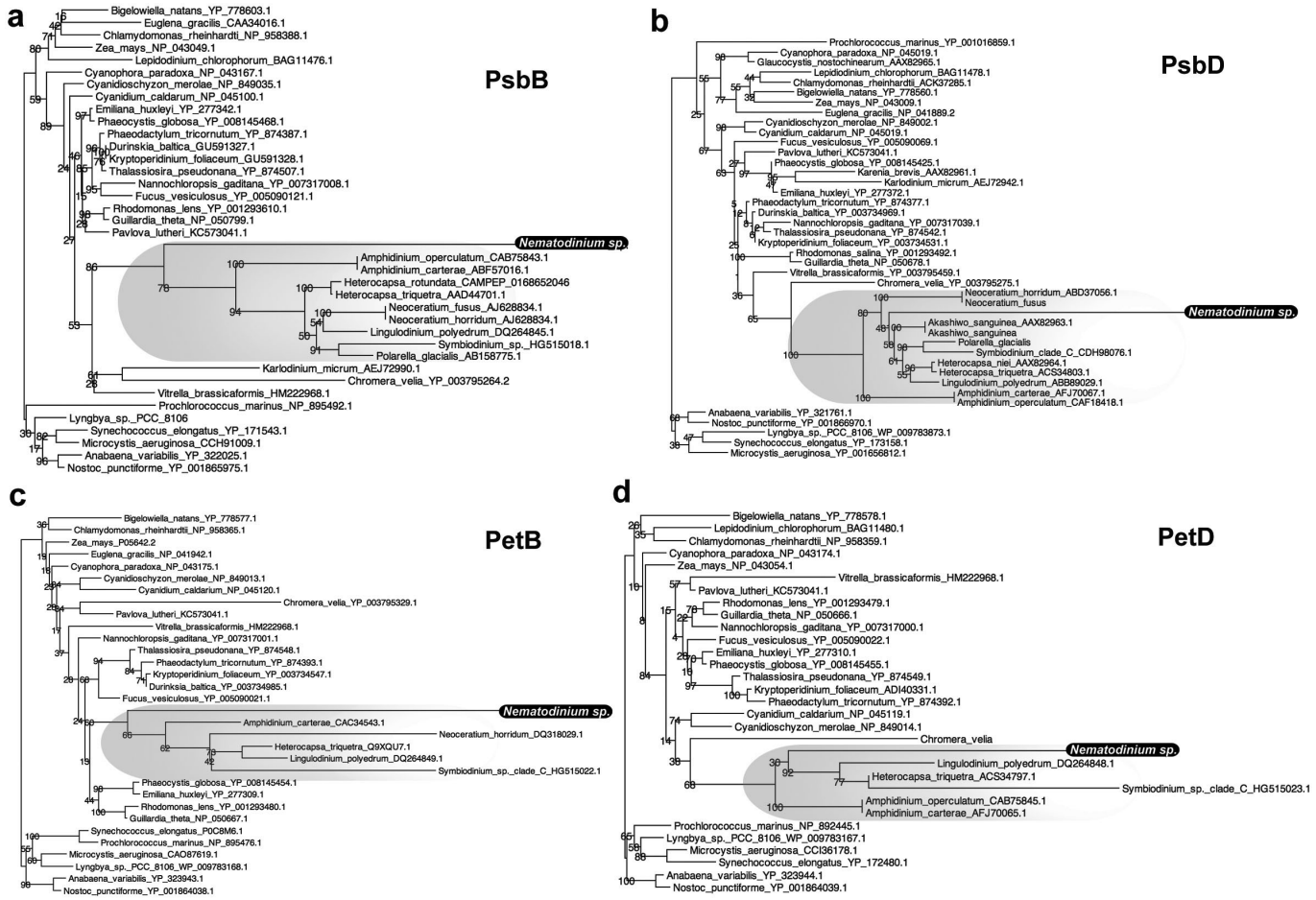

Extended Data Figure 7 | Individual photosystem protein trees. All the photosystem genes from *Nematodinium* sp. were amplified from the retinal body of the ocelloid. Support values for all phylogenies were calculated from 100 bootstraps using maximum likelihood analysis. **a**, Photosystem II CP47 (*PsbB*) protein phylogeny derived from a 504 AA alignment across 38 photosynthetic taxa. **b**, Photosystem II protein D1 (*PsbD*) phylogeny derived from a 342 AA alignment across 42 photosynthetic taxa. **c**, Cytochrome b_6 (*PetB*) protein phylogeny derived from a 216 AA alignment across 32 photosynthetic taxa. **d**, Cytochrome b_6/f complex subunit 4 (*PetD*) protein phylogeny derived from an 161 AA alignment across 31 photosynthetic taxa. Dinoflagellates are shaded in grey, and *Nematodinium* sp. is highlighted in black.

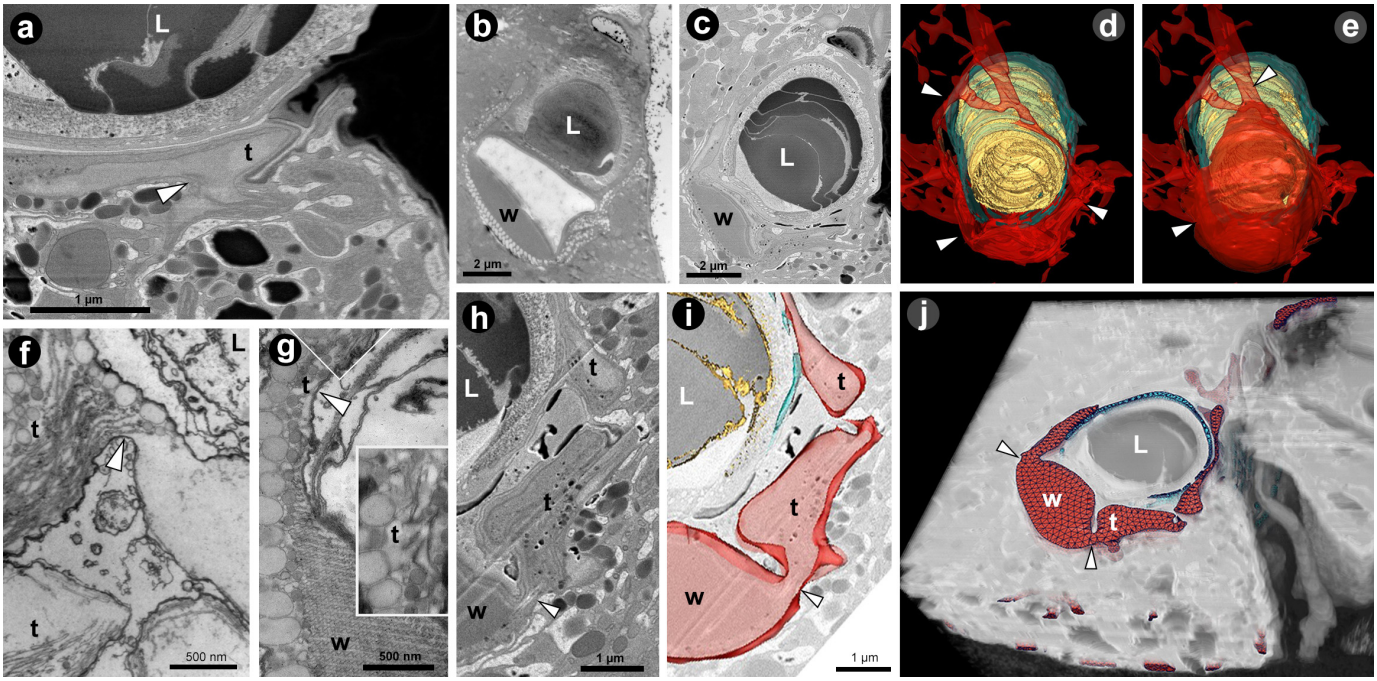

Extended Data Figure 8 | Continuity between the retinal body and the plastid network in *Nematodinium* sp. **a**, FIB-SEM slice of plastids attached to retinal body. **b**, TEM overview of ocelloid in a high-pressure frozen cell. **c**, FIB-SEM overview of ocelloid in a high-pressure frozen cell. **d**, Three-dimensional reconstruction of the ocelloid shown halved. **e**, Three-dimensional reconstruction of the ocelloid in full. **f**, Fusion site between plastids joined to the retinal body as seen in TEM. **g**, Site where the waveform-membrane region of the ocelloid joins to a region with thylakoids as seen in TEM. Inset shows thylakoids, and corresponds to the box in the main image. **h**, Fusion site as seen through FIB-SEM. **i**, Tracing of membrane continuity in Amira. **j**, Partial reconstruction of the ocelloid in Amira. Arrowheads point to fusion zones between sites bounded by the plastid membrane (reconstructed in red), blue denotes mitochondria, yellow denotes the surface of the lens. L, lens; w, waveform membranes; t, thylakoids.

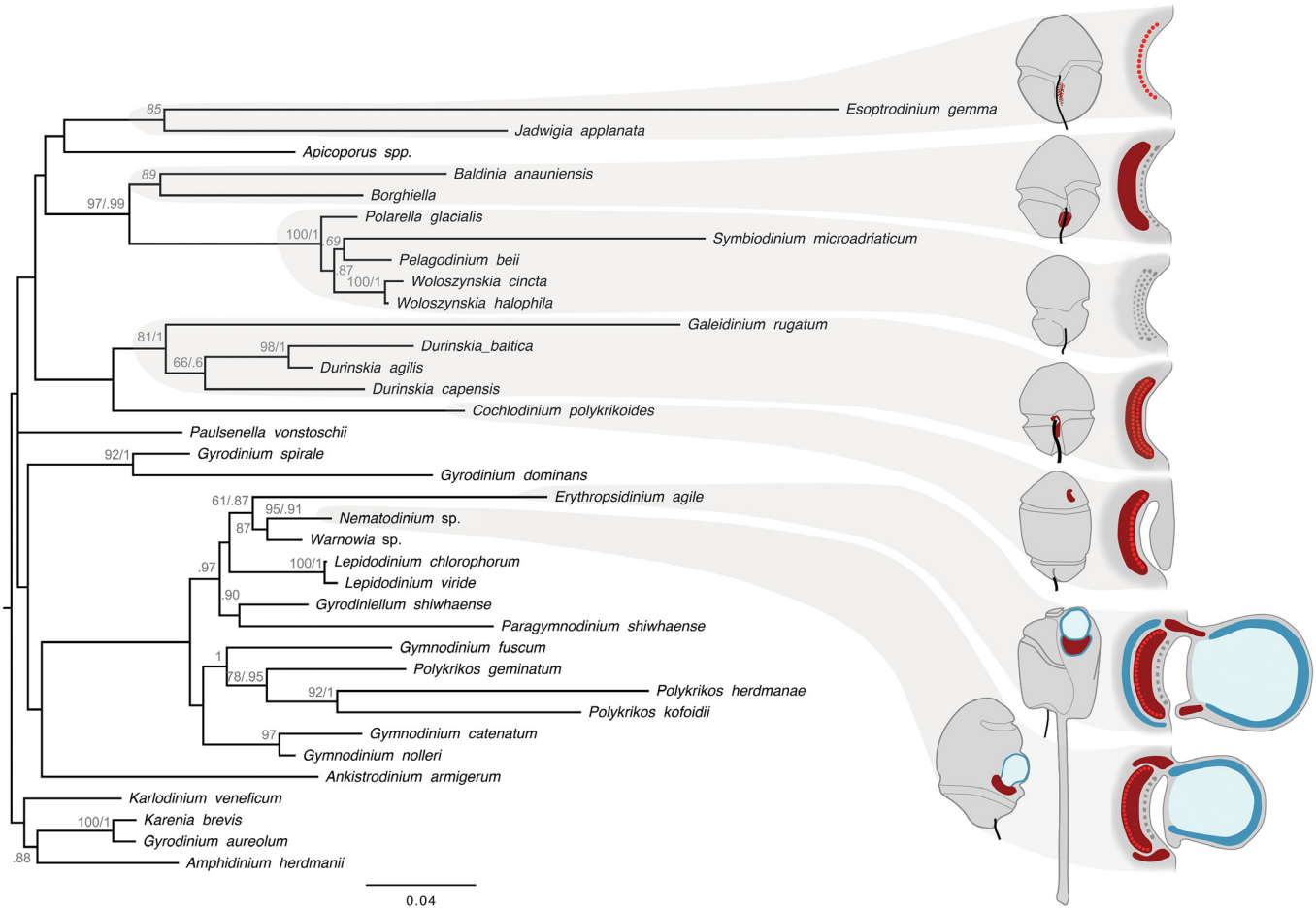

Extended Data Figure 9 | Dinoflagellate eyespot types within a phylogenetic context. Diagrams of whole cells and eyespots are shown for all dinoflagellates for which both ultrastructural descriptions and 18S and 28S ribosomal DNA sequences have been published. Eyespot diagrams highlight plastid-like structures (crimson), as well as mitochondria (dark blue), lens-like vesicles (light blue), lipid droplets (red dots), and crystalline layers (grey dashes). The phylogenetic tree was inferred from a 2,331-nucleotide alignment of concatenated 18S and 28S ribosomal DNA sequences across 36 genera; statistical support was evaluated with 500 bootstraps using maximum likelihood and 10,000 generations of Bayesian analysis. Bootstrap values above 60% are shown. For some taxa, 18S and 28S ribosomal sequences were concatenated from different species within the genus. Only the genus is shown for these taxa.

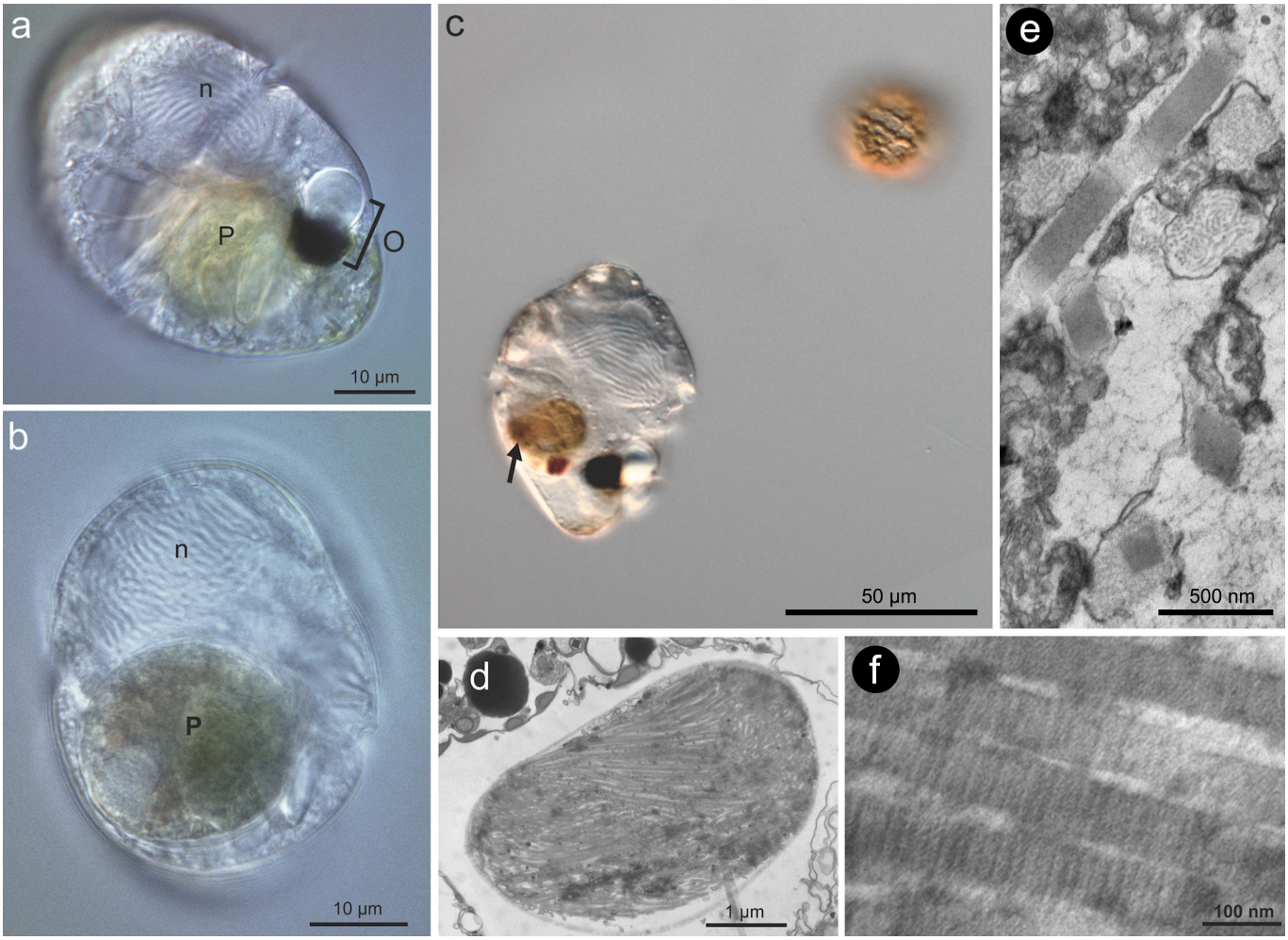

Extended Data Figure 10 | Light micrographs and TEM showing food vacuoles in *Nematodinium* sp. **a**, Differential interference contrast light micrographs showing a cell with prey (P) visible as green tinted food vacuole. **b**, Differential interference contrast light micrographs showing a cell in which the condensed dinoflagellate-type nuclei (n) are visible as birefringent chromosomes both in the predator and in the prey. **c**, Differential interference contrast light micrographs of a *Nematodinium* sp. cell containing digested prey (arrowhead) and co-occurring with potential prey, a smaller dinoflagellate. **d**, TEM showing a food vacuole inclusion consisting of a bolus of discharged trichocysts. **e**, TEM of undischarged dinoflagellate-type trichocysts showing their characteristic square shape in transverse section. **f**, TEM of discharged dinoflagellate-type trichocysts showing their characteristic striation pattern in longitudinal section.